ACS Photonics

pubs.acs.org/journal/apchd5

Article

Modulation of the Visible Absorption and Reflection Profiles of ITO Nanocrystal Thin Films by Plasmon Excitation

Michelle A. Blemker, Stephen L. Gibbs, Emily K. Raulerson, Delia J. Milliron, and Sean T. Roberts*

Cite This: *ACS Photonics* 2020, 7, 1188–1196

Read Online

ACCESS | Metrics & More | Article Recommendations | Supporting Information

ABSTRACT: Heavily doped metal oxide nanocrystals (NCs) possess tunable infrared localized surface plasmon resonances (LSPRs) that give them utility for several potential applications, including photothermal therapy, smart electrochromic windows, photocatalysis, and optical gating. However, studies of the photoresponse of these materials have largely been limited to the short-wave infrared (SWIR) spectral region, where their LSPR response peaks. Little has been done to study how LSPR excitation modulates the optical properties of these materials around their band gap in the UV/visible region. Here we demonstrate changes in the optical absorption and reflectivity of Sn-doped In_2O_3 (ITO) nanocrystal thin films following LSPR excitation. SWIR irradiation of ITO NCs substantially heats their free charge carriers, altering the NC film's dielectric response. This gives rise to an ultrafast increase in film reflectivity and absorptivity that relaxes within 1 ps following photoexcitation as hot charge carriers thermalize with the NC lattice. Using a model that accounts for free charge carrier behavior according to the Drude model as well as Fermi–Dirac statistics, we reproduce this behavior and predict that reflectivity changes of ~6% can be achieved via sufficient SWIR irradiation of ITO NC films. We also apply our model to other common plasmonic materials, highlighting that plasmonic metal oxide NC films can be used to obtain large, spectrally flat reflectivity changes throughout the visible region. Our results suggest these materials hold potential for use as terahertz optical gates and further our fundamental understanding of their plasmonic behavior.

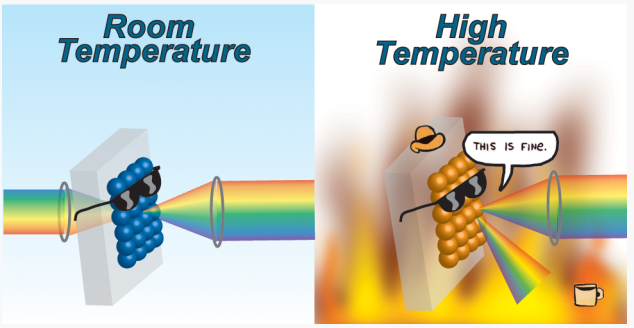

KEYWORDS: *infrared plasmonics, metal oxide nanocrystals, indium tin oxide, transient reflectivity, localized surface plasmon resonance, optical gating*

Metal nanoparticles are well-known for their ability to support localized surface plasmon resonances (LSPRs), which correspond to a collective response of the electrons within a particle driven by a time-varying external electric field.[1] LSPRs produce intense electric fields at the surface a particle, allowing them to act as nanoscale antennas to concentrate light into small volumes.[2−5] Exciting a particle's LSPR also produces hot carriers[6] that can drive catalytic transformations. If left unused, the energy of these carriers will be dissipated as heat to the particle's environment, which has applications for photothermal therapies and water purification.[5,7−10] Because of the growing utility of the short-wave infrared (SWIR) spectral region for telecom, photonics, and medical applications,[11−13] developing particles with LSPRs in this spectral region is highly desirable. However, creating metal particles that exhibit SWIR LSPRs is challenging, as the spectral position of a metal particle's LSPR is dependent on the square root of its free carrier concentration, n_e.[14] The high values of n_e for most metals place their LSPRs in the visible spectral range. While tuning nanoparticle aspect ratio or creating nanostructured arrays can yield metal structures with SWIR LSPRs,[15−18] these methods reduce the spatial density of high-electric-field hot spots and require precise shape control, which can be challenging to reproduce on a large scale.

Highly doped metal oxide nanocrystals (NCs) offer an alternative platform for plasmonically active SWIR materials. While metal oxide NCs are nominally wide-band-gap semiconductors, controlled doping of these materials via the introduction of vacancies, interstitial atoms, or aliovalent substitutional impurities can yield sufficient concentrations of free carriers to support LSPRs in the SWIR.[19−22] Metal oxide LSPRs can also be reversibly tuned via charge carrier addition through electrical and chemical means, leading to their investigation as electrochromic and photochromic materials for smart windows.[23−25] These materials offer additional promise as platforms for SWIR-fueled catalysis, chemical sensing, and photonic gating, but developing such applications

Received: December 25, 2019
Published: March 31, 2020

https://dx.doi.org/10.1021/acsphotonics.9b01825
ACS Photonics 2020, 7, 1188–1196

requires an improved understanding of how the optical properties of metal oxide NCs change under SWIR illumination.

While metal oxide NC LSPRs have been shown to exhibit optical responses similar to those of noble metal LSPRs upon illumination,[26−32] metal oxides possess semiconductor band gaps whose energies typically fall in the visible or near-UV spectral ranges. This gap creates the opportunity to produce unique optical responses unattainable with noble metal nanoparticles upon SWIR excitation. Prior work has shown that interband excitation of a metal oxide NC can shift its LSPR line shape by modulating its free carrier concentration.[28,31] However, the impact that intraband LSPR excitation, which heats a metal oxide NC's free electrons, has on its optical response near its band gap has attracted little attention. This is especially true for NC thin films, wherein SWIR excitation could be used to modulate a film's visible-to-UV transmission for photonics applications.

Here we report changes in the optical properties of Sn-doped In_2O_3 (ITO) NC thin films in the visible spectral range induced by LSPR excitation measured by ultrafast SWIR-pump, visible-probe transient absorption (TA) spectroscopy. We observe strong modulation of both the visible absorptivity and reflectivity of the films due to femtosecond heating of free electrons within the NCs' conduction band that alters their band gap and collective dielectric response. We reproduce these measured spectral changes with calculations based on a free electron model that accounts for Fermi−Dirac statistics. Photoinduced changes in the spectral response of ITO films diminish within 1 ps following LSPR excitation, a time scale commensurate with prior reports of ITO's hot-electron lifetime.[31−33] This rapid photoinduced change in both the absorptivity and reflectivity of the films, coupled with the ability to compositionally tune the optical properties of metal oxide NCs such as ITO over a wide spectral range, suggest these materials hold promise for a range of NIR-responsive applications, including photonic gates and optical sensors that can be switched at terahertz frequencies.

EXPERIMENTAL AND COMPUTATIONAL METHODS

ITO NC Synthesis. ITO NCs were synthesized by a slow-injection method first reported by the Hutchison group.[34] A mixture of tin(IV) acetate (Sigma-Aldrich) and indium(III) acetate (STREM, 99.99%) is mixed with oleic acid (Sigma-Aldrich, technical grade, 90%) at a concentration of 0.5 mmol of metal/mL of oleic acid. The mixture is degassed at 100 °C and then brought to 150 °C to react for a minimum of 2 h, during which time a metal−oleate complex forms. A syringe pump is used to inject this precursor solution into an excess volume of oleyl alcohol (13 mL) at 290 °C at a rate of 0.2 mL/min. To make the NCs whose dynamics are reported here, 2.5 mL of the oleate precursor was injected into a precursor solution containing the metal ions in a 1:9 Sn:In molar ratio.

NC Film Preparation and Characterization. To prepare NC films, an ITO NC dispersion with a concentration of 20 mg/mL was prepared in a solvent of 1:1 v/v hexane/octane, and 30 μL of this dispersion was spun on a quartz substrate at 1000 rpm for 60 s. ITO optical constants (n and k) were measured using ellipsometry of an ITO NC film spun-cast on silicon (J. A. Wollam M2000 spectroscopic ellipsometer). Extinction spectra were recorded with an Agilent Cary 5000 UV−vis−NIR spectrophotometer. To prevent reaction of the sample films with atmospheric oxygen or water vapor, ITO films used for transient absorption measurements were encapsulated under a nitrogen atmosphere using a second quartz substrate and epoxy resin placed at the film's edges.

Transient Absorption/Reflectivity Spectroscopy. Transient absorption and transient reflectivity measurements were completed using a 13.5 W, 3 kHz amplified Ti:sapphire laser with a center wavelength of 804 nm and a pulse length of ∼90 fs (Coherent Legend Elite Duo). Excitation pulses for ITO NCs were created by downconversion of ∼2.5 W of the Ti:sapphire output to 2000 nm using an optical parametric amplifier (Light Conversion TOPAS-Prime). Probe pulses were created by taking a portion of the fundamental output and focusing it into a 1 mm water flow cell to create a supercontinuum with a bandwidth of ∼350 nm to >800 nm. Probe light was dispersed spectrally using a 500 mm Czerny−Turner spectrometer (Acton Instruments SP2500 SpectraPro 2556-i) and collected with a CCD camera (Princeton Instruments PyLoN 100-BR). The polarizations of the pump and probe pulses used for TA measurements were parallel to one another. For transient reflectivity measurements, the pump and probe pulses were incident on sample films at an angle of 45° and had P polarization with respect to the sample surface.

Computational Modeling. All of the computational modeling was performed using home-built MATLAB scripts. When necessary, differential equations were integrated using MATLAB's ode45 solver, and fitting to experimental data was performed via the fitchisquare function.

EXPERIMENTAL RESULTS

The extinction spectrum of a 100 nm thick ITO NC film deposited on quartz is plotted in Figure 1. A broad peak

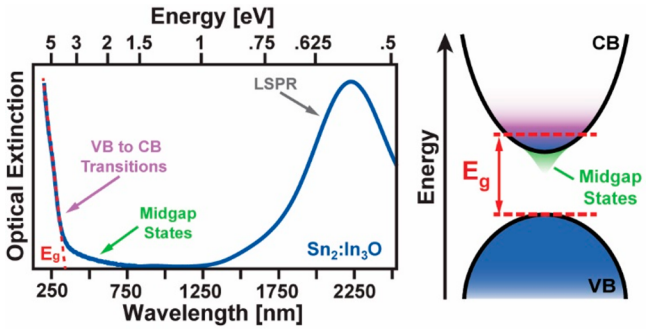

Figure 1. (left) Extinction spectrum of an ITO NC film. The sharp rise observed near 370 nm stems from ITO valence band to conduction band transitions, while the broad peak centered at 2200 nm arises from ITO's LSPR. A weak absorption tail extending from ∼370 to 800 nm is assigned to midgap transitions (right), as discussed in the text.

centered at 2220 nm (0.56 eV) can be assigned as the ITO LSPR (for a Drude model fit, see Figure S2). At higher energies near 370 nm (3.31 eV), the film's absorption spectrum rises sharply as a result of ITO valence band to conduction band transitions. Between this sharp rise and the onset of the LSPR absorption band, a weak absorption feature can be seen that extends from the rise of ITO's band gap (E_g) to wavelengths as long as 800 nm (1.55 eV). Debate exists regarding the origin of this broad absorption feature,[35−37] with the most prominent assignment being optical transitions involving midgap defect states. We will address this absorption

https://dx.doi.org/10.1021/acsphotonics.9b01825
ACS Photonics 2020, 7, 1188−1196

feature later within the context of our spectral model for the photoexcited dynamics of ITO NC films.

Figure 2A illustrates the impact of LSPR photoexcitation on the electron occupancy of states within the ITO conduction band. Following plasmon dephasing, the energy imparted by an exciting photon is thermalized among the free electrons within ITO's conduction band, elevating their temperature. Per Fermi–Dirac statistics, this increase in ITO's electronic temperature shifts the state occupancy within the conduction band toward high-energy states while reducing the population of low-energy states. This electronic heating of the ITO film has the net effect of shifting the absorption onset of its valence band to conduction band transitions to lower energy, as states near the film's conduction band minimum (CBM) occupied at room temperature are depopulated as a result of LSPR excitation (Figure 2B). This corresponds to a reversal of the Burstein–Moss effect, which describes the widening of ITO's band gap induced by doping of electrons into its conduction band.[38,39] This shift can be captured in a TA experiment, which tracks absorption gains induced by LSPR excitation. As hot electrons cool by transferring their energy to the ITO lattice via electron–phonon coupling, the shift in the ITO absorption onset is reversed, leading to a decay of the TA signal.

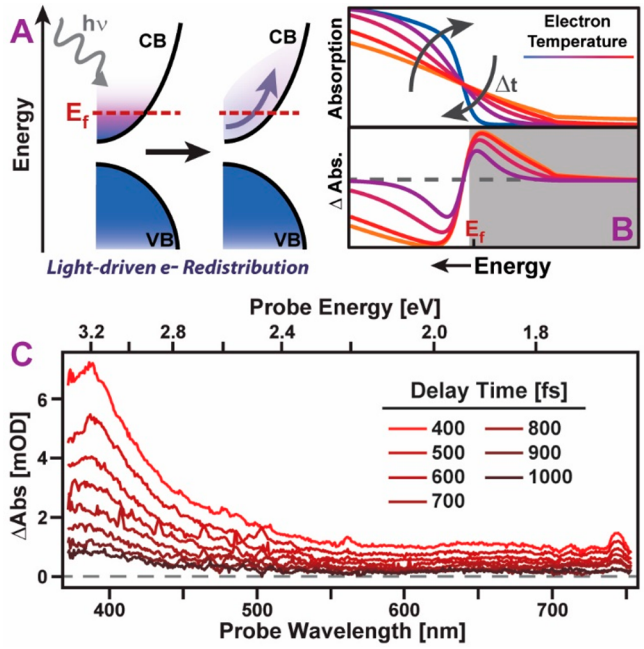

Figure 2. (A) LSPR excitation of an ITO NC rapidly heats its conduction band electrons, shifting their distribution about the NCs' Fermi energy. CB, conduction band; VB, valence band; E_f, Fermi energy. (B) Depopulation of states near the NCs' conduction band edge leads to a red shift of their valence band to conduction band absorption onset, as simulated by a spectral model (see the text) that accounts for photoinduced changes in the NCs' Fermi distribution and how this distribution evolves over time, Δt (top). This can be probed via TA, which measures differences in ITO absorption before and after LSPR excitation (simulated, bottom). (C) Experimental TA spectra of an ITO NC film measured following LSPR excitation at 2000 nm. Only the gain in absorption predicted in the shaded region in (B) is seen because of limitations of the probe range accessible by our TA system.

Figure 2C shows TA spectra measured following photoexcitation of the ITO NC film at 2000 nm (0.62 eV). As plasmon dephasing is anticipated to occur on a sub-100 fs time scale, which is on the order of our TA time resolution, we expect to observe the instantaneous rise of a hot electron population induced by the TA pump pulse. The TA spectra indeed show the appearance of a strong positive induced absorption near ITO's band gap (<400 nm) as well as an additional broad positive signal offset that extends throughout the visible region. In accordance with our predicted spectral signal (Figure 2B, shaded region), we assign the positive induced absorption peak near the ITO band gap to interband transitions that become available following electronic heating of ITO NCs by LSPR excitation. While a corresponding loss of absorption is predicted for probe wavelengths with energy exceeding the NC's Fermi energy, limitations of our probe source hinder our ability to fully examine this region. However, the TA data show a change in the curvature of the induced absorption band at ∼385 nm, which is expected near the ITO Fermi energy as predicted in Figure 2B.

Our data indicate that LSPR excitation creates a loss of population in electronic states close to the CBM that allows new transitions from the valence band into the conduction band. This lowers the effective optical band gap of the ITO NCs, reversing their Burstein–Moss shift. However, this lowering of the optical gap cannot fully account for the transient spectral dynamics we observe. A shift in ITO's conduction band occupancy due to heating of the NC's free electrons would be expected to produce an induced absorption near the NC's band gap that extends to energies only as low as the energy separation between the NC's valence band maximum and CBM (Figure 2A). However, we observe a weak photoinduced absorption that extends to probe energies as low as 1.65 eV (750 nm), which is significantly lower than the value we estimate for ITO's CBM (3.18 eV).[38] While it is conceivable that hybridization of Sn dopants with states within the In_2O_3 lattice can lower the CBM of ITO relative to undoped In_2O_3,[40] it is unlikely that such hybridization shifts this value by 1.59 eV, which would be needed to give rise to the photoinduced absorption tail we observe. This suggests a different effect underlies the dynamics that unfolds at low probe energies.

In a TA experiment, changes in the transmission (extinction) of a probe pulse induced by an excitation pulse are measured. While such changes are typically assigned to modulation of a sample's absorption profile, changes in a sample's reflectivity also impact TA spectra. As intraband excitation of an ITO NC film is not expected to increase its absorptivity at probe energies below the CBM, we speculated these changes could instead result from a change in the film's reflectivity. Indeed, prior studies of metal films reported reflectivity increases upon electron heating,[41,42] suggesting this mechanism could equally be at play in plasmonic ITO NC films.

To test this hypothesis, we recorded transient reflectivity spectra of an ITO NC film (Figure 3, top). Upon photoexcitation of the ITO LSPR, we indeed observe an increase in film reflectivity throughout much of the visible spectral range monitored by TA. This response decays on a time scale consistent with that observed in TA measurements, indicating the broad visible induced absorption band results from a photoinduced increase in film reflectivity. At shorter wavelengths (λ < 430 nm), a decrease in reflectivity is seen that

https://dx.doi.org/10.1021/acsphotonics.9b01825
ACS Photonics 2020, 7, 1188–1196

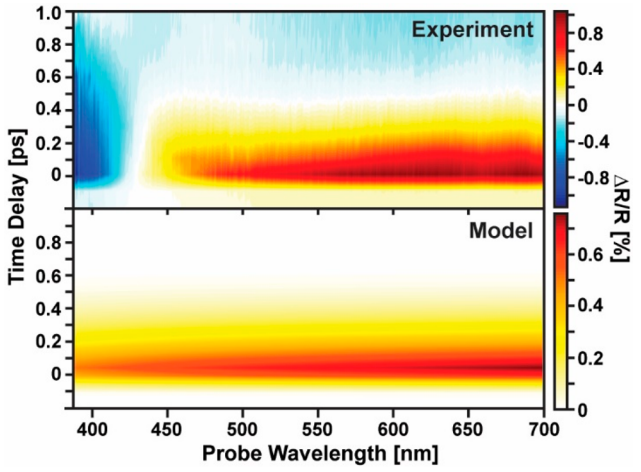

Figure 3. (top) Transient reflectivity spectra of an ITO NC film following excitation at 2000 nm. (bottom) Calculated transient reflectivity spectra of an ITO NC film based on a model that assumes instantaneous electronic heating of the film's conduction band electrons by an excitation pulse.

is consistent with an increase in ITO film absorptivity resulting from a reversal of the Burstein–Moss shift. Following the decay of the positive reflectivity change from 430 to 750 nm over ~0.5 ps, a weak decrease in reflectivity is seen throughout the visible spectral range that we attribute to heating of the NC lattice as a result of electron cooling. With knowledge that the photoinduced changes we observe at probe energies below the CBM are tied to an increase in ITO film reflectivity, we have developed a theoretical model that describes the temperature dependence of the absorption and reflectivity profiles of ITO NC films. This model shows that photoinduced heating of electrons within the film underlies the changes in its optical properties that we observe upon LSPR excitation.

THEORETICAL DESCRIPTION OF ITO NC FILM ABSORPTIVITY AND REFLECTIVITY

Using an approach based on the Drude model, we calculate the temperature-dependent reflectivity profile of an ITO NC film.

Table 1. Parameters Used to Compute the Transient Reflectivity and Absorptivity of an ITO NC Film following LSPR Excitation

parameter	value	method of determination
ε_∞	4	from ref 25
ω_p	14978 cm^{-1}	fit to the absorption spectrum
C_L	1.1418 J K^{-1} cm^{-3}	from ref 32
G_0	1.25 × 10^{10} J s^{-1} cm^{-3} K^{-1}	from ref 32
G_1	3.33 × 10^{7} J s^{-1} cm^{-3} K^{-2}	fit to TA spectra
γ	5.11 × 10^{-6} J K^{-2} cm^{-3}	from ref 32
η	1.14 × 10^{5} K^{-1}	fit to transient reflectivity data
Γ	1350 cm^{-1}	fit to the absorption spectrum

We start by using the two-temperature model (TTM)[26,32,43] to describe the temperature of the electrons within a photoexcited ITO NC. According to the TTM, excitation of a NC's LSPR creates a hot distribution of electrons within the NC's conduction band. These electrons then scatter off each other as well as off of phonons and point defects within the NC, lowering their temperature and raising that of the NC's phonon lattice until the two equilibrate. For ITO NCs, we

Table 2. Parameters Used to Compute the Transient Optical Extinction of an ITO NC Film following LSPR Excitation[a]

parameter	value	method of determination
E_f	3.31 eV	fit to TA data
E_c	3.18 eV	fit to TA data
γ_c	0.39 eV	fit to TA data
m_c/m_0	0.35	from ref 38
m_v/m_0	0.7	from ref 38

[a]The values of E_f and E_c are reported with respect to the valence band maximum, E_v, which is set to zero in our model.

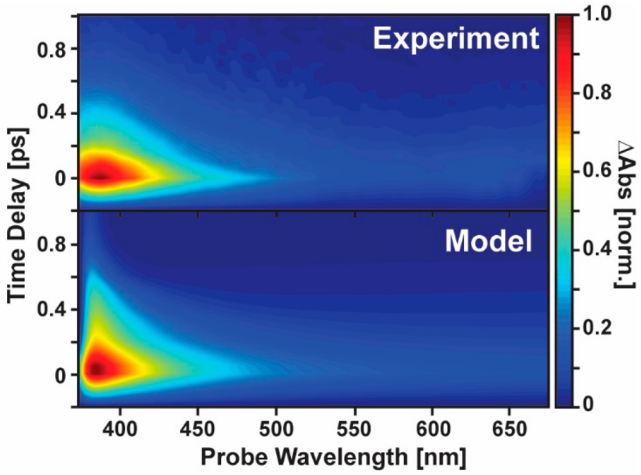

Figure 4. (top) Experimental TA spectrum of an ITO NC film following LSPR excitation and (bottom) the spectrum simulated using the model described in the text.

have previously used TA to characterize both the changes in their electronic temperature upon LSPR excitation and the time over which this temperature fully equilibrates with the ITO phonon lattice, finding this latter value to be <1 ps.[32] Following lattice heating, NC phonons excited by this process dissipate their energy to their environment over a few nanoseconds.

To describe photoinduced changes in the reflectivity profile of an ITO NC film, we start with the film's wavelength-dependent complex dielectric function, $\varepsilon(\omega)$, from the Drude model:[44]

$$\varepsilon(\omega) = \varepsilon_\infty - \frac{{\omega_p}^2}{\omega^2 + i\omega\Gamma} \quad (1)$$

where ω_p is the plasma frequency of NCs in the film, ε_∞ is the film's high-frequency dielectric constant, and Γ is a damping coefficient that describes plasmon dephasing. Importantly, $\varepsilon(\omega)$ is temperature-dependent, as it is altered by changes in the NC's electronic temperature, T_e. An increase in electronic temperature leads to a change in the NC's conduction band state occupancy, which impacts its dielectric environment and electron density. Likewise, Γ exhibits a dependence on the NC lattice temperature, T_L, since the number of electron scattering sites within the NC increases as its lattice warms. As the ITO lattice heat capacity is orders of magnitude larger than that of its electrons, optical absorption of a single photon negligibly heats the NC's lattice but can heat its electrons to a few thousand kelvins. For this reason and because our primary interest is in describing subpicosecond changes in the optical

https://dx.doi.org/10.1021/acsphotonics.9b01825
ACS Photonics 2020, 7, 1188–1196

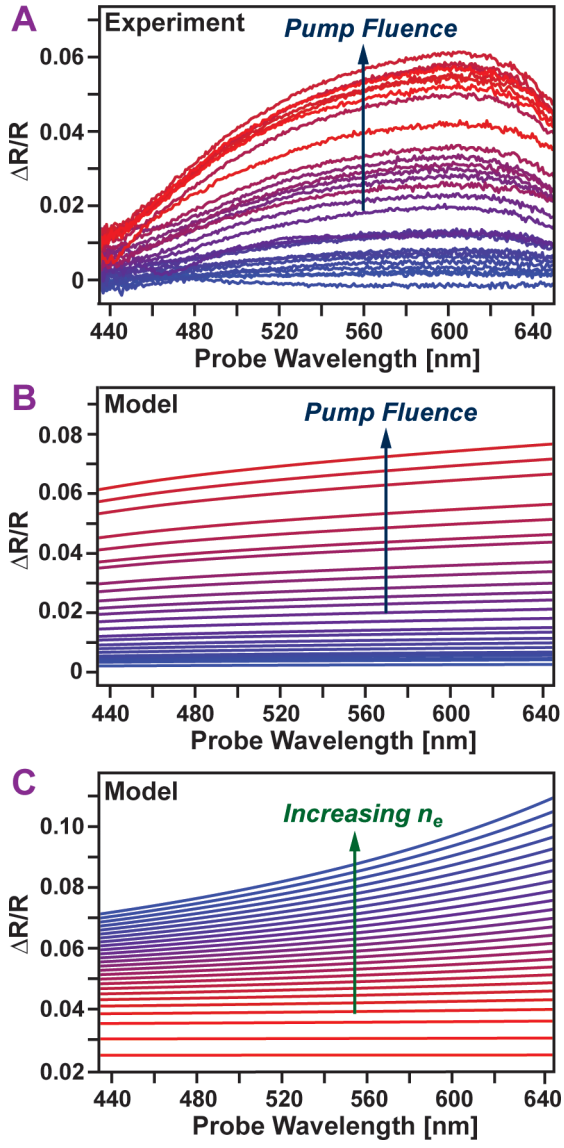

Figure 5. (A) Experimental $\Delta R/R$ for an ITO NC film at varying pump fluences. Fluence values range from 27 to 940 μJ/cm^2. (B) Calculated changes in ITO NC thin film reflectivity as a function of fluence at the same fluences used in (A). (C) Calculated changes in reflectivity based on an increase in carrier concentration at a set initial electronic temperature (15 000 K). The low and high carrier concentrations are 1×10^{19} cm^{-3} and 1×10^{21} cm^{-3} respectively.

properties of our NC films, we have chosen to neglect temperature-dependent changes in Γ in our model, focusing instead only on the impact that changing the electronic temperature has on the optical properties of ITO NC films.

Time-dependent changes in T_e and T_L can be obtained using the TTM:[6]

$$\gamma T_e \frac{dT_e}{dt} = -G(T_e - T_L) \tag{2a}$$

$$C_L \frac{dT_L}{dt} = G(T_e - T_L) \tag{2b}$$

where G is the electron−phonon coupling constant and γT_e and C_L are ITO's electron and phonon heat capacities, respectively. The time dependence of the NC film's electronic

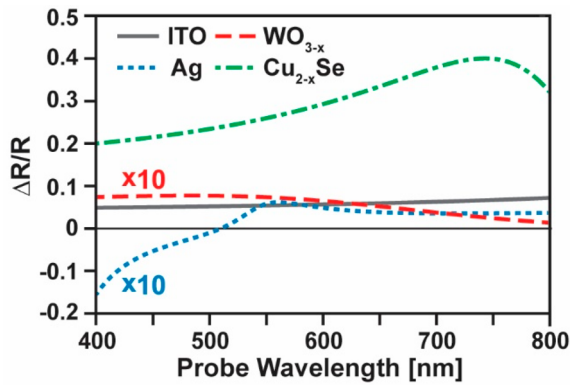

Figure 6. Calculated $\Delta R/R$ for thin films of different plasmonic NCs. Each film was modeled at a thickness of 200 nm, a volume fraction of 0.7, and an excitation fluence of 0.37 mJ/cm^2.

temperature modifies its dielectric function by altering ε_∞ according to

$$\varepsilon_\infty(T_e) = \varepsilon_{\infty,0} + \eta(T_e - T_0) \tag{3}$$

where $\varepsilon_{\infty,0}$ is the value of the high-frequency dielectric constant at the ambient temperature T_0 and η is a fitting parameter that denotes the lowest-order term in a Taylor series expansion describing the temperature dependence of ε_∞.[50] From eq 3, it is clear that changing the electronic temperature of an ITO film will alter its dielectric function, impacting how the film reflects and absorbs light. We note that prior authors have included terms up to a square variation of ε_∞ on T_e to model the plasmonic behavior of metallic and metal oxide NCs,[26,54] but we have found that only a linear expansion is needed to fully reproduce our ITO NC data.

With a description of the temperature dependence of the dielectric function in hand, we compute the reflectivity of the ITO NC film using

$$R = \left[\frac{(1-n)^2 + k^2}{(1+n)^2 + k^2}\right] \tag{4}$$

where the film's absorption coefficient, k, and index of refraction, n, are related to $\varepsilon(\omega)$ via

$$k = \sqrt{\frac{|\varepsilon| - \varepsilon_R}{2}} \tag{5a}$$

$$n = \sqrt{\frac{|\varepsilon| + \varepsilon_R}{2}} \tag{5b}$$

where ε_R is the real part of $\varepsilon(\omega)$.

Using eq 4 together with a description of the time-dependent changes in the electronic temperature of an ITO NC gleaned from the TTM (eq 2) and ellipsometry values for n and k (Figure S2), we compute the transient reflectivity response of an ITO NC film upon LSPR photoexcitation (Figure 3, bottom). Table 1 summarizes the constants used to compute this response. For simplicity, these calculations assumed that some properties of the ITO NC film, such as its lattice heat capacity and electron effective mass, are well-described by those of bulk ITO. Additionally, to fully reproduce the transient reflectivity signal, we needed to introduce a linear dependence of ITO's electron−phonon coupling constant on the electronic temperature, $G(T_e) = G_0 + G_1(T_e - T_0)$, as the excitation density used to record these

https://dx.doi.org/10.1021/acsphotonics.9b01825
ACS Photonics 2020, 7, 1188−1196

Table 3. Constants Used to Calculate the Reflectivity Changes Shown in Figure 5C

constant	ITO	WO_{3-x}	Ag	$Cu_{2-x}Se$
ω_p (cm^{-1})	14978[a]	33120[h]	69015[k]	35570[g]
ε_0	4[f]	6[i]	5[k]	10[g]
f_v	0.7	0.7	0.7	0.7
Γ (cm^{-1})	1350[a]	1254[c]	2054	3525[g]
γ (J cm^{-3} K^{-2})	5.11×10^{-6} [h]	5.5×10^{-5} [h]	6.51×10^{-5} [e]	3.2×10^{-6} [g]
C_L (J cm^{-3} K^{-1})	1.1418	3.03[j]	2.47[k]	2.72[g]
η (K^{-1})	1.14×10^{-5} [b]	2.65×10^{-5} [c]	2.1×10^{-4} [d,l]	8.4×10^{-5} [d,g]

[a]From a fit to the ITO absorption spectrum using the Drude model. [b]From a fit to the transient reflectivity of ITO films. [c]Approximations based on calculated line shapes and comparative properties of the other three materials. [d]Estimated by taking the square root of previously reported parameters that postulated a quadratic dependence of ε_∞ on T_e. [e]From ref 14. [f]From ref 25. [g]From ref 26. [h]From ref 32. [i]From ref 51. [j]From ref 52. [k]From ref 53. [l]From ref 54.

data produces high initial electronic temperatures (>10^4 K). This dependence agrees with prior work on plasmonic particles and metal films that noted changes in the electron−phonon coupling constant at elevated electronic temperature.[32,45] As we find that G_1 is positive for ITO, the rate of electron cooling is highest immediately upon photoexcitation and slows as ITO's conduction band electrons cool. The temperature dependence of G is discussed in depth in section SV in the Supporting Information.

Despite our simplifying assumptions, we find the transient reflectivity signal computed using this model reproduces many salient features of our experimental data. This calculation captures the broad reflectivity increase we observe experimentally for probe wavelengths above 430 nm, signifying that this change arises from electron heating of the NCs due to LSPR excitation. As the electrons equilibrate with the phonon lattice on a subpicosecond time scale, the reflectivity increase dissipates in accordance with our experimental data (Figure 3, top).

However, the current form of our model fails to capture two key aspects of the experimental data. First, the model does not reproduce the small negative offset seen at long times due to heating of the ITO NC lattice. This is expected, as we neglect reflectivity changes due to phonon heating. Second, the model does not capture the reflectivity decrease observed at shorter wavelengths (λ < 430 nm) for all pump−probe time delays. This too is expected, as the amplitude of our measured TA data markedly increases in this range (Figure 2C), suggesting the optical response of the ITO film in this spectral region reflects the appearance of a new photoinduced absorption. We have previously hypothesized this feature arises from a reversal of the Burstein−Moss shift due to electronic heating of the NC film upon LSPR excitation, which opens transitions to formerly occupied electron states near the NC conduction band edge.

To evaluate this latter hypothesis, we have modeled how the conduction band electron population changes upon heating using Fermi−Dirac statistics:[11]

$$f(E) = \frac{1}{\exp[(E - E_f)/k_B T_e] + 1} \tag{6}$$

where $f(E)$ is a Fermi function, with Fermi energy E_f, that describes the electron occupancy of states within the ITO conduction band. The ITO film absorption spectrum shown in Figure 1 exhibits a sharp increase in extinction around the optical band gap of our material (3.31 eV, 373 nm). There is also a broad absorption tail that extends from the band gap onset to longer wavelengths (300−800 nm) but ceases before reaching the LSPR absorption onset. Researchers have proposed several physical origins for this feature, including oxygen and indium vacancies, which introduce midgap states that give rise to an Urbach tail, or weakly absorbing transitions between states extending from the ITO valence and conduction band edges that have minimal oscillator strength or are dipole-forbidden as a result of ITO's crystal symmetry.[35,37] Describing each of these absorption features requires a model for ITO's band structure. Prior work on partially disordered semiconductors such as silicon has shown a piecewise-defined function describing the density of states (DOS) near a disordered semiconductor's CBM can reproduce well the absorption spectrum near the band gap.[46] This function pictures both the valence band and the conduction band to be parabolic, with a DOS that exhibits a square-root dependence on the energy, but adds to this DOS an exponential tail that describes defect states that extend into the semiconductor band gap:

$$N_c(E) = \frac{\sqrt{2}(m_c^*)^{3/2}}{\pi^2\hbar^3} \begin{cases} \sqrt{\frac{\gamma_c}{2}} \exp\left(-\frac{1}{2}\right) \exp\left(\frac{E - E_c}{\gamma_c}\right) & E \le E_c + \frac{\gamma_c}{2} \\ \sqrt{E - E_c} & E > E_c + \frac{\gamma_c}{2} \end{cases} \tag{7a}$$

where γ_c is a fitting parameter that determines the extent of the exponential tail in the conduction band, E_c is the CBM, and m_c^* is the effective mass of electrons in the conduction band. We assume the valence-band DOS, N_v, adopts a parabolic form near its band maximum, E_v:

$$N_v(E) = \frac{\sqrt{2}(m_v^*)^{3/2}}{\pi^2\hbar^3}\sqrt{E_v - E} \tag{7b}$$

where m_v^* is the effective mass of carriers in the valence band. The product of the Fermi function and the DOS at a specific temperature gives us the density of filled and empty electron states at a given energy E. To model ITO's absorption line shape, we compute the probability of having a filled and empty state separated by a specific energy.

With this model in hand, we use the TTM to compute changes in the Fermi distribution of ITO NCs following LSPR excitation and time-dependent changes in their optical spectra as their electrons cool. We combine these changes in absorption with our calculated reflectivity changes to compute the time variation of an ITO NC film's extinction for comparison with TA spectra. Section SIV provides a detailed

https://dx.doi.org/10.1021/acsphotonics.9b01825
ACS Photonics 2020, 7, 1188−1196

description of how we combine the computed absorption and reflectivity changes to fit our TA spectra. As a part of this process, the values of E_f, E_σ, and γ_c were floated as fitting parameters, and the best-fit values are reported in Table 2.

Figure 4 compares the results of this model to our experimental TA spectra. Despite our model's simplicity, it reproduces many salient features of our data, capturing both the spectral variation of the TA line shape and its time-dependent decay. Examining the values extracted from the model for E_c and E_f, we find they are in accordance with prior estimates for ITO NCs featuring dopant concentrations similar to those examined here.[47] The value recovered for γ_σ 0.39 eV, suggests much of the induced absorption we observe between the CBM (3.18 eV, 390 nm) and the rise of the reflectivity response (430 nm; Figure 3A) stems from midgap states that reside near the CBM. Given the high surface-to-volume ratio of our ITO NCs, structural defects generated near NC surfaces provide a plausible explanation for the appearance of these states. We also note a shortcoming of our model: it underestimates the strength of the room-temperature midgap state absorption highlighted in Figure 1. One potential explanation for this is that midgap states extending from the valence band may also be present and could contribute to the NC film's ground-state absorption. However, we find that modeling of our TA spectra did not require introduction of valence band midgap states, suggesting that if these states are indeed present, optical transitions involving them are not impacted by LSPR excitation.

Importantly, the magnitude of the NC film's reflectivity change upon LSPR excitation is non-negligible (~1% peak $\Delta R/R$; Figure 3), which together with its rapid rise upon SWIR illumination and dissipation following SWIR light removal suggests ITO NC films may hold promise as SWIR-gated optical switches for photonics. Previous work has shown doped semiconductor NCs can exhibit ultrafast reflectivity changes (<1 ps), some reaching above 80%. However, these studies were limited to the SWIR and NIR and were measured near or at the center of the material's LSPR maximum,[29,48,49] making it unclear how the absorption and reflectivity profiles of these materials respond in the visible spectral range.

To explore the use of ITO NC films for broadband visible switching, we proceeded to vary the temperature of the electrons within the ITO NC film by increasing the intensity of the SWIR laser source used to photoexcite it. Figure 5A plots the TR signal of an ITO NC film deposited on quartz measured 150 fs following photoexcitation as a function of the SWIR pump fluence. Figure 5B shows the change in reflectivity predicted by our model at these same fluences. We find the films' reflectivity saturates at a fluence of 600 $\mu J/cm^2$, which yields a $\Delta R/R$ value of ~6% at a probe wavelength of 600 nm. Below this value, the films' reflectivity increases linearly with increasing excitation density (Figure S6), reflecting the dependence of ε_∞ on the electronic temperature in our model. The slight downturn in the reflectivity profile at wavelengths longer than 600 nm likely stems from broadening of the films' LSPR line shape due to lattice heating, which is not described by our model; this could in part explain the reflectivity saturation.

Compositional tuning of ITO NCs offers a potential way to further enhance this photoinduced response. To explore this, we use the Maxwell–Garnet EMA dielectric approximation[44] to model the carrier concentration dependence of the dielectric function of ITO NC films:

$$\frac{\varepsilon_{eff} - \varepsilon_M}{\varepsilon_{eff} + 2\varepsilon_M} = f_v \left[\frac{\varepsilon_p(\omega) - \varepsilon_M}{\varepsilon_p(\omega) + 2\varepsilon_M} \right] \quad (8)$$

where ε_{eff} is the effective dielectric function of the ITO NC film, ε_M is the dielectric constant of the medium surrounding the NCs within the film, which we take to be described by the properties of oleate ligands bound to their surface, f_v is the NC volume fraction within the film, and $\varepsilon_p(\omega)$ is the frequency-dependent dielectric function of bulk ITO. We find our model predicts shifting the NC's LSPR closer to the visible range by increasing the free carrier concentration via doping provides a complementary method to increase the ITO NC film's reflectivity upon electronic heating (Figure 5C) that could be used to obtain reflectivity changes approaching 10%.

To compare the photoinduced reflectivity changes of ITO NC films to those achievable for films composed of other nanocrystalline plasmonic materials, in Figure 6 we plot the $\Delta R/R$ values computed using our model for ITO NC films against the corresponding reflectivity changes calculated for $Cu_{2-x}Se$, Ag, and WO_{3-x} NC solids. In making this comparison, we assume that each film is composed of an identical volume fraction of NCs and that the NCs' free electrons are heated by an instantaneous incident energy flux of 0.37 mJ/cm^2 from photons whose frequency matches the peak of each material's LSPR. Details regarding these calculations, including sources of physical constants used to model each material, can be found in Table 3.

Looking at the computed reflectivity changes, we find both Ag and WO_{3-x} exhibit vanishingly small reflectivity changes in the visible region. This reflects their high electronic heat capacities relative to ITO, which results in comparatively lower electronic temperatures upon LSPR excitation.[32] In contrast, $Cu_{2-x}Se$ is predicted to exhibit a stronger reflectivity change than ITO in the visible spectral range because it possesses both a lower electronic heat capacity than ITO and an LSPR that peaks at the red edge of the visible spectral range. However, while the magnitude of its reflectivity change is larger, $Cu_{2-x}Se$'s plasmon and band gap absorption features tail into the visible region.[26,48] This may make this material suboptimal for applications that require broadband switching between reflective and transmissive states for visible light. In contrast, ITO is transparent in the visible region at room temperature and displays a comparatively flat reflectivity change across the visible spectral range, suggesting its suitability for applications requiring a broad, spectrally neutral response. This response can be further enhanced with consideration of device design, such as creating multiple ITO–quartz bilayers that can continually reflect as light transmits through the system.

CONCLUSIONS

We have characterized changes in the optical absorption and reflectivity profiles of ITO NC films in the visible spectral range following LSPR excitation by NIR light. The majority of this optical response decays in less than 1 ps through equilibration between hot electrons and the NC lattice. Such rapid decay indicates these materials hold great promise for use as switches for NIR and visible photonic circuits and other technologies that require optical gating at terahertz switching rates. We find the photoinduced changes in the absorption and reflectivity of ITO NC films can be well-described by a model that accounts for how the films' optical constants respond to electron heating induced by LSPR excitation. Using this model,

https://dx.doi.org/10.1021/acsphotonics.9b01825
ACS Photonics 2020, 7, 1188–1196

we predict reflectivity changes of ~6% can be reasonably obtained. We also find ITO's visible reflectivity profile remains spectrally flat as its electrons are heated, which stands out among plasmonic NC materials, making a case for ITO's use for broadband photonics applications.

■ ASSOCIATED CONTENT

Supporting Information

The Supporting Information is available free of charge at https://pubs.acs.org/doi/10.1021/acsphotonics.9b01825.

STEM images of ITO NCs showing their size dispersion, ITO NC absorption line shape modeling using the Drude model, ellipsometry data used to compute ITO NC film optical constants, expanded discussion of the model for ITO physical parameters and transient absorption and transient reflection lineshapes, and description of the temperature dependence of ITO's electron−phonon coupling constant and high-frequency dielectric constant, ε_∞ (PDF)

■ AUTHOR INFORMATION

Corresponding Author

Sean T. Roberts − *Department of Chemistry, The University of Texas at Austin, Austin, Texas 78712, United States;* orcid.org/0000-0002-3322-3687; Email: roberts@cm.utexas.edu

Authors

Michelle A. Blemker − *Department of Chemistry, The University of Texas at Austin, Austin, Texas 78712, United States*

Stephen L. Gibbs − *McKetta Department of Chemical Engineering, The University of Texas at Austin, Austin, Texas 78712, United States;* orcid.org/0000-0003-2533-0957

Emily K. Raulerson − *Department of Chemistry, The University of Texas at Austin, Austin, Texas 78712, United States*

Delia J. Milliron − *McKetta Department of Chemical Engineering, The University of Texas at Austin, Austin, Texas 78712, United States;* orcid.org/0000-0002-8737-451X

Complete contact information is available at: https://pubs.acs.org/10.1021/acsphotonics.9b01825

Notes

The authors declare no competing financial interest.

■ ACKNOWLEDGMENTS

M.A.B., E.K.R., and S.T.R. acknowledge support from the National Science Foundation (CHE-1610412), the Robert A. Welch Foundation (Grant F-1885), and the Research Corporation for Science Advancement via a Cottrell Scholars Award (Grant 24489). M.A.B. also acknowledges funding support from a University of Texas at Austin Provost Excellence Fellowship. D.J.M. acknowledges support from the National Science Foundation (CHE-1905263) and the Robert A. Welch Foundation (Grant F-1848), and S.L.G. was supported by a National Science Foundation Graduate Fellowship (DGE-1610403). The authors also acknowledge the Texas Materials Institute for use of facilities for ellipsometry, vapor deposition, and electron microscopy.

■ REFERENCES

(1) Willets, K. A.; Van Duyne, R. P. Localized Surface Plasmon Resonance Spectroscopy and Sensing. *Annu. Rev. Phys. Chem.* **2007**, *58*, 267−297.

(2) Anker, J. N.; Hall, W. P.; Lyandres, O.; Shah, N. C.; Zhao, J.; Van Duyne, R. P. Biosensing with Plasmonic Nanosensors. *Nat. Mater.* **2008**, *7*, 442−453.

(3) Hutter, E.; Fendler, J. H. Exploitation of Localized Surface Plasmon Resonance. *Adv. Mater.* **2004**, *16*, 1685−1706.

(4) Mayer, K. M.; Hafner, J. H. Localized Surface Plasmon Resonance Sensors. *Chem. Rev.* **2011**, *111*, 3828−3857.

(5) Jain, P. K.; Huang, X.; El-Sayed, I. H.; El-Sayed, M. A. Noble Metals on the Nanoscale: Optical and Photothermal Properties and Some Applications in Imaging, Sensing, Biology, and Medicine. *Acc. Chem. Res.* **2008**, *41*, 1578−1586.

(6) Fann, W. S.; Storz, R.; Tom, H. W. K.; Bokor, J. Direct Measurement of Nonequilibrium Electron-Energy Distributions in Subpicosecond Laser-Heated Gold Films. *Phys. Rev. Lett.* **1992**, *68*, 2834−2837.

(7) Dongare, P. D.; Alabastri, A.; Pedersen, S.; Zodrow, K. R.; Hogan, N. J.; Neumann, O.; Wu, J.; Wang, T.; Deshmukh, A.; Elimelech, M. L.; Li, Q.; Nordlander, P.; Halas, N. J. Nanophotonics-Enabled Solar Membrane Distillation for Off-Grid Water Purification. *Proc. Natl. Acad. Sci. U. S. A.* **2017**, *114*, 6936−6941.

(8) Wang, S.; Riedinger, A.; Li, H.; Fu, C.; Liu, H.; Li, L.; Liu, T.; Tan, L.; Barthel, M. J.; Pugliese, G.; De Donato, F.; Scotto D'Abbusco, M.; Meng, X.; Manna, L.; Meng, H.; Pellegrino, T. Plasmonic Copper Sulfide Nanocrystals Exhibiting Near-Infrared Photothermal and Photodynamic Therapeutic Effects. *ACS Nano* **2015**, *9*, 1788−1800.

(9) Boerigter, C.; Aslam, U.; Linic, S. Mechanism of Charge Transfer from Plasmonic Nanostructures to Chemically Attached Materials. *ACS Nano* **2016**, *10*, 6108−6115.

(10) Wu, K.; Chen, J.; McBride, J. R.; Lian, T. Efficient Hot-Electron Transfer by a Plasmon-Induced Interfacial Charge-Transfer Transition. *Science* **2015**, *349*, 632−635.

(11) Kriegel, I.; Scotognella, F.; Manna, L. Plasmonic Doped Semiconductor Nanocrystals: Properties, Fabrication, Applications and Perspectives. *Phys. Rep.* **2017**, *674*, 1−52.

(12) Law, S.; Adams, D. C.; Taylor, A. M.; Wasserman, D. Mid-infrared Designer Metals. *Opt. Express* **2012**, *20*, 12155−12165.

(13) Zhu, Z.; Zou, Y.; Hu, W.; Li, Y.; Gu, Y.; Cao, B.; Guo, N.; Wang, L.; Song, J.; Zhang, S.; Gu, H.; Zeng, H. Near-Infrared Plasmonic 2D Semimetals for Applications in Communication and Biology. *Adv. Funct. Mater.* **2016**, *26*, 1793−1802.

(14) Ashcroft, N. W.; Mermin, N. D. *Solid State Physics*; Brooks/Cole, 1976.

(15) Sau, T. K.; Rogach, A. L.; Jäckel, F.; Klar, T. A.; Feldmann, J. Properties and Applications of Colloidal Nonspherical Noble Metal Nanoparticles. *Adv. Mater.* **2010**, *22*, 1805−1825.

(16) Bukasov, R.; Shumaker-Parry, J. S. Highly Tunable Infrared Extinction Properties of Gold Nanocrescents. *Nano Lett.* **2007**, *7*, 1113−1118.

(17) Le, F.; Brandl, D. W.; Urzhumov, Y. A.; Wang, H.; Kundu, J.; Halas, N. J.; Aizpurua, J.; Nordlander, P. Metallic Nanoparticle Arrays: A Common Substrate for Both Surface-Enhanced Raman Scattering and Surface-Enhanced Infrared Absorption. *ACS Nano* **2008**, *2*, 707−718.

(18) Atwater, H. A.; Polman, A. Plasmonics for Improved Photovoltaic Devices. *Nat. Mater.* **2010**, *9*, 205−213.

(19) Agrawal, A.; Cho, S. H.; Zandi, O.; Ghosh, S.; Johns, R. W.; Milliron, D. J. Localized Surface Plasmon Resonance in Semiconductor Nanocrystals. *Chem. Rev.* **2018**, *118*, 3121−3207.

(20) Manthiram, K.; Alivisatos, A. P. Tunable Localized Surface Plasmon Resonances in Tungsten Oxide Nanocrystals. *J. Am. Chem. Soc.* **2012**, *134*, 3995−3998.

(21) Ye, X.; Fei, J.; Diroll, B. T.; Paik, T.; Murray, C. B. Expanding the Spectral Tunability of Plasmonic Resonances in Doped Metal-

Oxide Nanocrystals through Cooperative Cation-Anion Codoping. *J. Am. Chem. Soc.* **2014**, *136*, 11680−11686.
(22) Lounis, S. D.; Runnerstrom, E. L.; Llordes, A.; Milliron, D. J. Defect Chemistry and Plasmon Physics of Colloidal Metal Oxide Nanocrystals. *J. Phys. Chem. Lett.* **2014**, *5*, 1564−1574.
(23) Runnerstrom, E. L.; Llordés, A.; Lounis, S. D.; Milliron, D. J. Nanostructured Electrochromic Smart Windows: Traditional Materials and NIR-Selective Plasmonic Nanocrystals. *Chem. Commun.* **2014**, *50*, 10555−10572.
(24) Liang, X.; Guo, C.; Chen, M.; Guo, S.; Zhang, L.; Li, F.; Guo, S.; Yang, H. A Roll-to-Roll Process for Multi-Responsive Soft-Matter Composite Films Containing Cs_xWO_3 Nanorods for Energy-Efficient Smart Window Applications. *Nanoscale Horiz.* **2017**, *2*, 319−325.
(25) Hamberg, I.; Granqvist, C. G. Evaporated Sn-doped In_2O_3 Films: Basic Optical Properties and Applications to Energy-Efficient Windows. *J. Appl. Phys.* **1986**, *60*, R123−R160.
(26) Scotognella, F.; Della Valle, G.; Srimath Kandada, A. R.; Dorfs, D.; Zavelani-Rossi, M.; Conforti, M.; Miszta, K.; Comin, A.; Korobchevskaya, K.; Lanzani, G.; Manna, L.; Tassone, F. Plasmon Dynamics in Colloidal $Cu_{2-x}Se$ Nanocrystals. *Nano Lett.* **2011**, *11*, 4711−4717.
(27) Luther, J. M.; Jain, P. K.; Ewers, T.; Alivisatos, A. P. Localized Surface Plasmon Resonances Arising from Free Carriers in Doped Quantum Dots. *Nat. Mater.* **2011**, *10*, 361−366.
(28) Diroll, B. T.; Guo, P.; Chang, R. P. H.; Schaller, R. D. Large Transient Optical Modulation of Epsilon-Near-Zero Colloidal Nanocrystals. *ACS Nano* **2016**, *10*, 10099−10105.
(29) Guo, P.; Schaller, R. D.; Ketterson, J. B.; Chang, R. P. H. Ultrafast Switching of Tunable Infrared Plasmons in Indium Tin Oxide Nanorod Arrays with Large Absolute Amplitude. *Nat. Photonics* **2016**, *10*, 267−273.
(30) Kriegel, I.; Urso, C.; Viola, D.; De Trizio, L.; Scotognella, F.; Cerullo, G.; Manna, L. Ultrafast Photodoping and Plasmon Dynamics in Fluorine-Indium Codoped Cadmium Oxide Nanocrystals for All-Optical Signal Manipulation at Optical Communication Wavelengths. *J. Phys. Chem. Lett.* **2016**, *7*, 3873−3881.
(31) Tice, D. B.; Li, S.-Q.; Tagliazucchi, M.; Buchholz, D. B.; Weiss, E. A.; Chang, R. P. H. Ultrafast Modulation of the Plasma Frequency of Vertically Aligned Indium Tin Oxide Rods. *Nano Lett.* **2014**, *14*, 1120−1126.
(32) Johns, R. W.; Blemker, M. A.; Azzaro, M. S.; Heo, S.; Runnerstrom, E. L.; Milliron, D. J.; Roberts, S. T. Charge Carrier Concentration Dependence of Ultrafast Plasmonic Relaxation in Conducting Metal Oxide Nanocrystals. *J. Mater. Chem. C* **2017**, *5*, 5757−5763.
(33) Guo, P.; Schaller, R. D.; Ocola, L. E.; Diroll, B. T.; Ketterson, J. B.; Chang, R. P. H. Large Optical Nonlinearity of ITO Nanorods for Sub-Picosecond All-Optical Modulation of the Full-Visible Spectrum. *Nat. Commun.* **2016**, *7*, 12892.
(34) Jansons, A. W.; Hutchison, J. E. Continuous Growth of Metal Oxide Nanocrystals: Enhanced Control of Nanocrystal Size and Radial Dopant Distribution. *ACS Nano* **2016**, *10*, 6942−6951.
(35) King, P. D. C.; Veal, T. D.; Fuchs, F.; Wang, Ch. Y.; Payne, D. J.; Bourlange, A.; Zhang, H.; Bell, G. R.; Cimalla, V.; Ambacher, O.; Egdell, R. G.; Bechstedt, F.; McConville, C. F. Band Gap, Electronic Structure, and Surface Electron Accumulation of Cubic and Rhombohedral In_2O_3. *Phys. Rev. B: Condens. Matter Mater. Phys.* **2009**, *79*, 205211.
(36) Walsh, A.; Da Silva, J. L. F.; Wei, S.-H.; Körber, C.; Klein, A.; Piper, L. F. J.; DeMasi, A.; Smith, K. E.; Panaccione, G.; Torelli, P.; Payne, D. J.; Bourlange, A.; Egdell, R. G. Nature of the Band Gap of In_2O_3 Revealed by First-Principles Calculations and X-Ray Spectroscopy. *Phys. Rev. Lett.* **2008**, *100*, 167402.
(37) Ho, C.-H.; Chan, C.-H.; Tien, L.-C.; Huang, Y.-S. Direct Optical Observation of Band-Edge Excitons, Band Gap, and Fermi Level in Degenerate Semiconducting Oxide Nanowires In_2O_3. *J. Phys. Chem. C* **2011**, *115*, 25088−25096.
(38) Hamberg, I.; Granqvist, C. G.; Berggren, K.-F.; Sernelius, B. E.; Engström, L. Band-gap Widening in Heavily Sn-doped In_2O_3. *Phys. Rev. B: Condens. Matter Mater. Phys.* **1984**, *30*, 3240−3249.
(39) Irmscher, K.; Naumann, M.; Pietsch, M.; Galazka, Z.; Uecker, R.; Schulz, T.; Schewski, R.; Albrecht, M.; Fornari, R. On the Nature and Temperature Dependence of the Fundamental Band Gap of In_2O_3. *Phys. Status Solidi A* **2014**, *211*, 54−58.
(40) Berggren, K.-F.; Sernelius, B. E. Band-gap Narrowing in Heavily Doped Many-Valley Semiconductors. *Phys. Rev. B: Condens. Matter Mater. Phys.* **1981**, *24*, 1971−1986.
(41) Schoenlein, R. W.; Lin, W. Z.; Fujimoto, J. G.; Eesley, G. L. Femtosecond Studies of Nonequilibrium Electronic Processes in Metals. *Phys. Rev. Lett.* **1987**, *58*, 1680−1683.
(42) Hohlfeld, J.; Müller, J. G.; Wellershoff, S.-S.; Matthias, E. Time-resolved Thermoreflectivity of Thin Gold Films and its Dependence on Film Thickness. *Appl. Phys. B: Lasers Opt.* **1997**, *64*, 387−390.
(43) Ekici, O.; Harrison, R. K.; Durr, N. J.; Eversole, D. S.; Lee, M.; Ben-Yakar, A. Thermal Analysis of Gold Nanorods Heated with Femtosecond Laser Pulses. *J. Phys. D: Appl. Phys.* **2008**, *41*, 185501.
(44) Mendelsberg, R. J.; Garcia, G.; Li, H.; Manna, L.; Milliron, D. J. Understanding the Plasmon Resonance in Ensembles of Degenerately Doped Semiconductor Nanocrystals. *J. Phys. Chem. C* **2012**, *116*, 12226−12231.
(45) Lin, Z.; Zhigilei, L. V.; Celli, V. Electron-Phonon Coupling and Electron Heat Capacity of Metals Under Conditions of Strong Electron-Phonon Nonequilibrium. *Phys. Rev. B: Condens. Matter Mater. Phys.* **2008**, *77*, 075133.
(46) O'Leary, S. K.; Johnson, S. R.; Lim, P. K. The Relationship Between the Distribution of Electronic States and the Optical Absorption Spectrum of an Amorphous Semiconductor: An Empirical Analysis. *J. Appl. Phys.* **1997**, *82*, 3334−3340.
(47) Zandi, O.; Agrawal, A.; Shearer, A. B.; ReImnitz, L. C.; Dahlman, C. J.; Staller, C. M.; Milliron, D. J. Impacts of Surface Depletion on the Plasmonic Properties of Doped Semiconductor Nanocrystals. *Nat. Mater.* **2018**, *17*, 710−717.
(48) Wei, R.; Tian, X.; Luo, H.; Liu, M.; Yang, Z.; Luo, Z.; Zhu, H.; Guo, H.; Li, J.; Qiu, J. Heavily Doped Semiconductor Colloidal Nanocrystals as Ultra-Broadband Switches for Near-Infrared and Mid-Infrared Pulse Lasers. *ACS Appl. Mater. Interfaces* **2019**, *11*, 40416−40423.
(49) Yang, Y.; Kelley, K.; Sachet, E.; Campione, S.; Luk, T. S.; Maria, J.-P.; Sinclair, M. B.; Brener, I. Femtosecond Optical Polarization Switching Using a Cadmium Oxide-Based Perfect Absorber. *Nat. Photonics* **2017**, *11*, 390−395.
(50) Del Fatti, N.; Vallée, F.; Flytzanis, C.; Hamanaka, Y.; Nakamura, A. Electron Dynamics and Surface Plasmon Resonance Nonlinearities in Metal Nanoparticles. *Chem. Phys.* **2000**, *251*, 215−226.
(51) Viswanathan, K.; Brandt, K.; Salje, E. Crystal Structure and Charge Carrier Concentration of $W_{18}O_{49}$. *J. Solid State Chem.* **1981**, *36*, 45−51.
(52) Adachi, M.; Akishige, Y.; Asahi, T.; Deguchi, K.; Gesi, K.; Hasebe, K.; Hikita, T.; Ikeda, T.; Iwata, Y.; Komukae, M.; Mitsui, T.; Nakamura, E.; Nakatani, N.; Okuyama, M.; Osaka, T.; Sakai, A.; Sawaguchi, E.; Shiozaki, Y.; Takenaka, T.; Toyoda, K.; Tsukamoto, T.; Yagi, T. Oxides · WO_3, M2. In *Ferroelectrics and Related Substances · Oxides*; Shiozaki, Y., Nakamura, E., Mitsui, T., Eds.; Landolt-Börnstein - Group III Condensed Matter, Vol. *36A2*; Springer: Berlin, 2002.
(53) Hodak, J. H.; Martini, I.; Hartland, G. V. Spectroscopy and Dynamics of Nanometer-Sized Noble Metal Particles. *J. Phys. Chem. B* **1998**, *102*, 6958−6967.
(54) Owens, D. T.; Fuentes-Hernandez, C.; Hales, J. M.; Perry, J. W.; Kippelen, B. A Comprehensive Analysis of the Contributions to the Nonlinear Optical Properties of Thin Ag Films. *J. Appl. Phys.* **2010**, *107*, 123114.

https://dx.doi.org/10.1021/acsphotonics.9b01825
ACS Photonics 2020, 7, 1188−1196